



Universiteit  
Leiden  
The Netherlands

## **Computational electrocatalysis: methods and fundamental applications on CO<sub>2</sub> reduction and formic acid oxidation**

Granda Marulanda, L.P.

### **Citation**

Granda Marulanda, L. P. (2021, October 19). *Computational electrocatalysis: methods and fundamental applications on CO<sub>2</sub> reduction and formic acid oxidation*. Retrieved from <https://hdl.handle.net/1887/3217519>

Version: Publisher's Version

License: [Licence agreement concerning inclusion of doctoral thesis in the Institutional Repository of the University of Leiden](#)

Downloaded from: <https://hdl.handle.net/1887/3217519>

**Note:** To cite this publication please use the final published version (if applicable).



Oudenhofmolen  
Oegstgeest, The Netherlands

# 3

## A SIMPLE METHOD TO CALCULATE SOLUTION-PHASE FREE ENERGIES OF CHARGED SPECIES IN COMPUTATIONAL ELECTROCATALYSIS

Calculating the adsorption potentials of ions with density functional theory and comparing across various ions requires an accurate reference energy of the ion in solution and electrons at the same electrochemical scale. Here we highlight a previously used method for determining the reference free energy of solution phase ions using a simple electrochemical thermodynamic cycle, which allows this free energy to be calculated from that of a neutral gas-phase or solid species and an experimentally measured equilibrium potential, avoiding the need to model solvent around the solution phase ion in the electronic structure calculations. While this method is not new, we describe its use and utility in detail and show that this same method can be used to find the free energy of any ion from any reaction, as long as the half-cell equilibrium potential is known, even for reactions that do not transfer the same number of protons and electrons. To illustrate its usage, we compare the adsorption potentials obtained with DFT of  $I^*$ ,  $Br^*$ ,  $Cl^*$ , and  $SO_4^{*}$  on Pt(111) and Au(111), and  $OH^*$  and  $Ag^*$  on Pt(111) with those measured experimentally and find that this simple and computationally affordable method reproduces the experimental trends.

---

*This chapter is based on Granda-Marulanda, L. P.; McCrum, I. T.; Koper, M. T. M. A Simple Method to Calculate Solution-Phase Free Energies of Charged Species in Computational Electrocatalysis. J. Phys.: Condens. Matter* **2021**, 33 (20), 204001.

### 3.1 Introduction

Elucidation and understanding of the complex structure at the electrochemical interface, between electrolyte, adsorbates, and electrode, is one of the main fundamental problems in electrochemistry/electrocatalysis. The advancement of in situ spectroscopic and imaging techniques has allowed fundamental information at the atomic and molecular level to be obtained.<sup>1-9</sup> In addition, the increase of computational power has allowed computational tools based on the generalized gradient approximation (GGA) Density Functional Theory (DFT) to provide predictions complementary to experimental results, based on the computed adsorption energetics, thermodynamics, and kinetics of processes at the electrochemical interface.<sup>10-15</sup>

Among the main computational challenges that first-principles DFT simulations face at present are (i) the description of the potential dependence of the electrochemical processes and (ii) the description of the solvated species (protons and charged species) in the bulk solution phase and the description of these same species at the metal-electrode interface. In the first case, the biggest limitation is that the methods available to simulate variations of the electrode potential dependence are computationally more expensive than the traditional simulations, due to the necessity of changing the charge during the simulation to keep the potential constant.<sup>16-18</sup>

In periodic simulations, where plane-wave basis sets are used, calculating negatively charged species by adding charges to a small supercell can lead to unphysical energies. This is due to the so-called "charge leakage", which are non-wanted interactions with the next periodic representation of the system, and also because of the unphysical distribution of the charge in the cell due to improper screening.<sup>19</sup>

To address this, periodic DFT models have been devised to simulate charged systems, by adding a background charge to make the system charge neutral but with the extra requirement of an energy correction afterwards.<sup>20-22</sup> Similarly, it has also been proposed to add background charge with a dielectric continuum to prevent charge transfer.<sup>23</sup> Recently, Tölle et al.,<sup>24</sup> suggested a method to calculate ionization potentials of liquid water in periodic systems, where the finite charge subsystem is embedded and surrounded by an extended subsystem, obtaining comparable results of the ionization potential with experimental data and continuum dielectric models.

The other difficulty faced by DFT simulations is the description of solvated species. The calculated energies within the DFT framework represent systems in the gas phase (or vacuum) at 0 K, instead of systems in solution phase as they are in an electrochemical environment. In general, models that are meant to capture solvation effects in electrochemistry, including explicit solvation,<sup>25-32</sup> implicit solvation<sup>33-38</sup> or a combination of the two,<sup>39-41</sup> add significant computational expense to the calculation due to the long length and time scales of the solvation structure and dynamics. Explicit solvation is modelled by adding solvent molecules in the simulation cell, where the solvent structure can be based on periodic electronic-structure calculations using GGA-DFT, ab initio molecular dynamics (AIMD), or classical molecular dynamics.<sup>42-44</sup> Implicit solvation is modelled as a dielectric continuum as described by the experimentally measured bulk dielectric constant and is a model that is in active development and

improvement.<sup>45–47</sup> These solvation models can be applied to both solvation in the bulk solution and at the electrode-adsorbate-electrolyte interface. Even though much effort has been devoted to accurately compute solvation energies of protons and ions in solution,<sup>48–54</sup> by combining thermodynamic cycles with implicit continuum models,<sup>53,55,56</sup> or by calculating the solvation energy of charged species, either with implicit or explicit solvation, the subject remains a challenging part of computational electrochemistry.<sup>57,58</sup>

Fortunately, for ions in bulk solution, thermodynamic cycles can be very practical because they provide free energies of charged species in solution by relating the exact free energy of a solution-phase ion to that of a readily and accurately calculated neutral gas-phase or solid-state species, for instance by using experimental redox potentials. Such thermodynamic cycles allow solution-phase free energies to be calculated without the need to model the solvent.

One such thermodynamic cycle which has gained standard, widespread use in computational electrochemistry is the “computational hydrogen electrode” (CHE),<sup>59</sup> in which the free energy of a proton-electron pair is related to that of hydrogen gas,  $H_{(aq)}^+ + e^- \rightleftharpoons \frac{1}{2}H_{2(g)}$ , by the definition of the equilibrium potential of the standard or reversible hydrogen electrode (RHE). At a potential of 0 V vs RHE and standard conditions of 1 bar, and 298.15 K, the proton-electron pair ( $H^+ + e^-$ ) is in equilibrium with hydrogen gas  $H_{2(g)}$ , allowing the free energy of the proton-electron pair to be calculated from neutral  $\frac{1}{2}H_{2(g)}$ . This method allows for the thermodynamics of reactions involving coupled proton-electron transfers to be calculated easily and accurately using DFT.

Many similar thermodynamic cycles have been used to calculate the free energy of solution-phase ions other than protons. Calle-Vallejo et al. used experimentally measured formation energies of liquid nitric acid and the aqueous nitrate anion and the DFT calculated free energy of nitric acid in the gas phase to calculate the free energy of the nitrate anion in aqueous solution to examine its adsorption thermodynamics.<sup>60</sup> In a recent study, McCrum et al.<sup>61</sup> used two different methods to calculate the free energy of halide anions in solution, so that the thermodynamics of their adsorption to an electrode surface could be determined. In the first method, the energy of the halide anion in vacuum was calculated using DFT, then it was corrected to the aqueous electrolyte by adding on an experimentally measured solvation energy, similar to the method used by Yeh et al.<sup>62</sup> To then convert the energy of the ion-electron couple from an absolute scale to the normal hydrogen electrode scale, a second experimental value is needed, the absolute (vacuum) potential of the hydrogen electrode at standard state (4.4 V).<sup>63</sup> In the second method, the authors used an approach similar to that of the computational hydrogen electrode, relating the free energy of the aqueous halide anions to that of the gas-phase halogens using their experimentally measured standard reduction potentials. This latter method is also described by Hansen et al.<sup>64</sup> to study chlorine evolution and Gossenberger et al.<sup>65</sup> to construct phase diagrams of halides co-adsorbed with hydrogen on platinum.

In another investigation to determine the likelihood of co-adsorption of  $ClO_4^*$  and  $Cl^*$  with  $OH^*$  on Pt(111),<sup>66</sup> the authors used the same method to calculate the free energy of  $ClO_4^-(aq)$  and  $Cl^-(aq)$ . In this latter method, the half-cell equilibrium potentials of the redox couples of  $(Cl_2(g) / Cl^-(aq))$  and  $(ClO_4^-(aq), H^+ / Cl_2(g))$ , and the calculated free energies of  $Cl_2(g)$  and  $H_2O(l)$  are needed. The final solution-phase free energy of the anions,  $ClO_4^-(aq)$  and  $Cl^-(aq)$  is then corrected to their initial experimental concentrations, using the Nernst equation, also similar to the

work described by Gossenberger et al.<sup>67</sup> Additionally, various studies have discussed the relevance of thermodynamic cycles often combined with an implicit continuum model to determine solvation energies to calculate  $pK_a$ 's and reduction potentials.<sup>68,55,53,56,69–71</sup>

Therefore, using standard redox potentials to obtain solvation energies or vice versa through thermodynamic cycles is well known, and while many thermodynamic cycles can and have been defined, there is a need to re-visit and illustrate the potential of this conceptually simple, computationally efficient, and transferable method to calculate the reference free energy of any solution-phase ion, in bulk electrolyte, far from the electrode surface. Resources containing thousands of redox reactions, such as the standard thermodynamic tables of equilibrium potentials,<sup>72,73</sup> are available, and so it is very likely that the species of interest are tabulated there.

In this *Chapter*, we describe how the free energy of any solvated ion can be calculated from that of a neutral gas-phase or solid-state species and an experimentally measured equilibrium potential, eliminating the need to model solvation for the bulk solution-phase species with DFT. We show that, in combination with the computational hydrogen electrode, this method works even for half-cell reactions which involve an unequal number of protons and electrons.<sup>74</sup> This is of fundamental importance because achieving robust predictions with computational modelling depends on the choice of the reference state. A solution phase reference state is necessary, for example, for the computation of specific adsorption potentials of ions on electrodes.<sup>61,64–66</sup> The interactions between adsorbed ions, the solvent, and reaction intermediates, are of significant importance in catalysis and electrocatalysis, as they can modify bond breaking/formation, adsorption energies, and consequently reaction pathways<sup>75–83</sup> important for catalyst design.

Since this method relies on the experimentally measured equilibrium potential, we could argue that it is less “ab initio” than the CHE, thus we are limited to the availability of suitable experimental data and need to be aware of the accuracy of the experimentally measured potentials. However, the advantages are (i) that it facilitates the calculation of the free energies of various ions at the same potential scale, which is the scale at which the equilibrium potential sits, and (ii) similar to the CHE, there is no increase in the computational intensity of the calculations, as the calculations rely on neutral gas-phase species. We show examples of how to calculate solution free energies of ions in the context of computational electrocatalysis, and finally demonstrate how this method can be used by using DFT to examine the thermodynamics of adsorption of  $I^*$ ,  $Br^*$ ,  $Cl^*$ , and  $SO_4^{*}$  on Pt(111) and Au(111), and  $OH^*$  and  $Ag^*$  on Pt(111) and comparing with those measured experimentally.

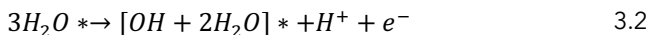
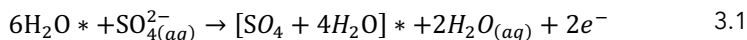
## 3.2 Methods

In this section, we first describe the method for calculating the free energy of an ion in solution, and then apply this method to calculate the adsorption free energy of  $Cl^*$ ,  $Br^*$ ,  $I^*$ , and  $SO_4^{*}$  on Pt(111) and Au(111), and  $OH^*$  and  $Ag^*$  on Pt(111).

### 3.2.1 Computational Details

The Vienna Ab Initio Simulation Package (VASP)<sup>84-86</sup> was used to perform the DFT calculations, using a plane-wave basis set and the Projector Augmented Wave approach.<sup>87,88</sup> The cut-off energy for the basis set was 450 eV. The Perdew-Burke-Ernzerhof, (PBE), exchange-correlation functional was used.<sup>89,90</sup> Both the Pt(111) and Au(111) surfaces were modeled as a 4 layer slab (or 5 layer slab, in the case of  $\text{SO}_4^*$  on Au(111) and Pt(111)), with the bottom 2 layers frozen at the experimentally measured lattice constants of 3.92 Å and 4.08 Å (as a first approximation), respectively,<sup>91</sup> in a  $3 \times 3$  unit cell. A Monkhorst-Pack mesh k-space sampling grid<sup>92</sup> of  $5 \times 5 \times 1$  and  $8 \times 8 \times 1$  were used for Pt(111) and Au(111), respectively. To simulate the surfaces, a vacuum spacing larger than 14 Å between the slabs was set. Dipole corrections were included in the surface-normal direction.<sup>93</sup> Structural optimization was performed until the forces on each atom were below 0.02 eV Å<sup>-1</sup>. The adsorption thermodynamics for each adsorbate were evaluated at 1/9 monolayer (ML) coverage.  $\text{OH}^*$  and  $\text{SO}_4^*$  were additionally simulated with co-adsorbed explicit water molecules to approximate the near-surface solvation effect on the adsorption energy.

For sulfate adsorption, see Eq. 3.1, a  $6\text{H}_2\text{O}^*$  water bilayer was used as the reactant state and two water molecules were displaced upon  $\text{SO}_4^*$  adsorption, giving a product state with 4 water molecules co-adsorbed with  $\text{SO}_4^*$ . For  $\text{OH}^*$ , see Eq. 3.2, the reference state was three hydrogen-bonded water molecules adsorbed on the surface ( $3\text{H}_2\text{O}^*$ ), one proton was then removed to create the product state, which was two water molecules co-adsorbed with  $\text{OH}^*$ . While the water adsorbed on the surface in the initial state, and the water remaining on the surface, co-adsorbed with the adsorbate in the product state, were static, and only vibrational entropy changes were considered, the adsorption reaction does include the entropy change associated with the adsorbate displacing adsorbed water molecules into bulk solution (2 water molecules displaced for  $\text{SO}_4^*$ , 1 for  $\text{OH}^*$ ). Additional entropy changes of the solvent near the surface are not considered. This method of modeling the effects of near-surface solvent therefore only approximates the change in entropy upon adsorption. This method also captures only the most local solvating enthalpic interactions, such as hydrogen bonding to the adsorbate and static dipole screening, approximating what could be considered part of the first “solvation shell” around the adsorbate and surface.



Silver adsorption on Pt(111) was examined at a coverage of 1 and 2 ML, in a  $1 \times 1$  Pt(111) unit cell, with a  $9 \times 9 \times 1$  k-space grid. Single gas-phase molecules are calculated in a large box of (15 Å  $\times$  15 Å  $\times$  15 Å), with a k-point grid of  $1 \times 1 \times 1$ . The 0 K DFT energy of metallic silver is calculated using a slab model, instead of a 3-d bulk structure. We varied the slab thickness (above the thickness where the energy of the slab is converged) of a Ag(111)  $1 \times 1$  unit cell, where the slope of a

line fit to the energy versus slab thickness represents the energy of bulk silver, per bulk atom. This slab method allows for a greater cancellation of errors than with a 3-d bulk structure.<sup>94</sup> The slabs were symmetric, with the middle two layers frozen at the experimentally measured lattice constant.

All free energies of the gas-phase species are calculated following Eq. 3.3 given further below, at 298.15 K and 1 atm of pressure, except for liquid water, which is calculated at its experimentally measured partial pressure at 298.15 K, where basically its gas-phase entropy is corrected by -0.0887 eV.<sup>59,95</sup> SO<sub>2</sub> (aq) was taken as the free energy of SO<sub>2</sub>(g) as correction by its solvation energy (-0.005 eV)<sup>96</sup> does not significantly changes the energy. The work function was determined as the difference between the Fermi energy and the one electron potential in vacuum,  $\Phi = V - E_{fermi}$ . The partial charges were determined with the AIM Bader analysis,<sup>97,98</sup> using the Bader program from Henkelman's group.<sup>99</sup>

The free energy of the solution (aqueous) phase anion is calculated following the method we describe in the following section. Briefly, we use a tabulated value of the experimentally measured equilibrium potential connecting a neutral gas-phase (see Figure 3.1) or solid-state species, with the aqueous-phase ion of interest from which the adsorption energies or potentials are calculated. For I, Br, and Cl, this reaction was the reduction from solid I<sub>2</sub> and gas-phase Br<sub>2</sub> and Cl<sub>2</sub>, which at standard state have equilibrium potentials of 0.620, 1.094, and 1.36 V vs SHE.<sup>72</sup> The free energy of solid-phase iodine was calculated as that of gas-phase iodine at a partial pressure equal to its vapor pressure at room temperature.<sup>100</sup> For SO<sub>4</sub><sup>2-</sup>, this reaction was that of sulfur dioxide reduction, see Eq. 3.9, with an equilibrium potential at standard state of 0.158 V vs SHE.<sup>72</sup> For Ag<sup>+</sup>, the free energy of the aqueous silver cation was calculated from that of metallic silver, with an equilibrium potential of 0.799 V vs SHE.<sup>72</sup> For each reaction, the experimentally measured equilibrium potential at standard state was obtained from the data in "Standard Electrode Potentials and Temperature Coefficients in Water at 298.15K".<sup>72</sup> Lastly, for OH\*, the free energy of adsorption was calculated relative to hydrogen gas and water, following the computational hydrogen electrode method, CHE,<sup>59</sup> with a standard equilibrium potential of exactly 0 V vs SHE.

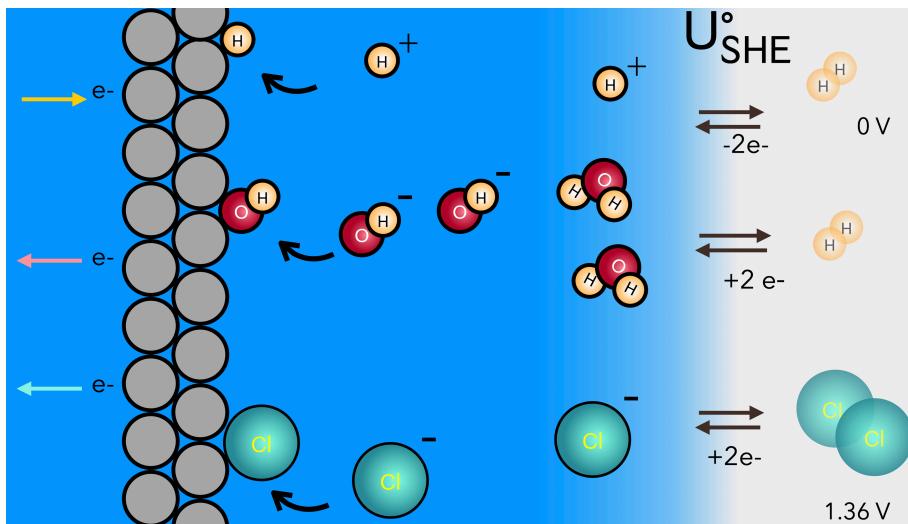


**FIGURE 3.1**

Representation of ions ( $Cl^-$ ,  $OH^-$ ,  $H^+$ ), in solution phase in equilibrium with gas-phase species at their experimentally measured equilibrium potentials, except for  $OH^-$ ,<sup>72</sup> (right), and same ions adsorbed on a generic electrode with 111 facet (left). The reference neutral species for adsorbed  $OH^*$  are  $H_2O(l)$  and  $H_2(g)$  using the CHE at 0 V vs SHE.

### 3.2.2 Determination of the free energy of ions in solution

The accuracy of the energy of the solution-phase ion using thermodynamic cycles depends on how well DFT can represent the neutral species. Therefore, it is crucial to include gas-phase corrections<sup>101–103</sup> or solid-phase corrections<sup>104</sup> to the neutral species from which the ion solution free energy will be calculated. For instance, if one is interested in the solution-phase free energy of oxalic acid, although a neutral species, its solution-phase free energy can be calculated from  $CO_2(g)$  and its equilibrium redox potential  $2CO_2(g) + 2H^+ + 2e^- \rightarrow H_2C_2O_4$ , ( $CO_2(g)$ ,  $H^+/H_2C_2O_4$ ,  $U_{SHE}^\circ = -0.432$  V). In this case, the calculated DFT energy of  $CO_2(g)$  will require a gas-phase correction that is functional dependent.

The free energy of the gas-phase species  $X(g)$  can then be determined with DFT and statistical mechanics following Eq. 3.3

$$G_{X(g)} = E_{DFT} + ZPE + E_{int} - TS + PV \quad 3.3$$

where ZPE is the zero-point vibrational energy,  $E_{int}$  includes the vibrational, rotational, and translational contributions (above 0 K) to the internal energy, and S is the entropy of the gas-phase molecule. The internal energy is calculated using statistical mechanics for vibrational, rotational, and translational energy, while

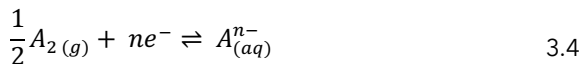
the entropy, in this *Chapter*, is taken from standard thermodynamic tables,<sup>73</sup> PV is the pressure-volume contribution to the free energy, obtained as  $PV = Nk_B T$  where  $N = 1$  mole,  $k_B$  is the Boltzmann constant and  $T$  is the temperature.

In this *Chapter*, for the solid-state species, the 0 K DFT energy is taken as an approximation of the free energy of the solid at room temperature. In the following, we show how to obtain the free energy of solution-phase ions from gas-phase species. The first step is to identify a reaction that links the charged species we are interested in with a neutral species that is ideally in the gas phase or in the solid phase, and has a known (experimentally measured) equilibrium potential (which can be found, for example, in the electrochemical series, tabulated for many ions).<sup>72,73</sup> For example, if we want to determine the aqueous free energy of  $\text{Cl}_{(\text{aq})}^-$ , we can use its standard half-cell reduction reaction,  $\frac{1}{2}\text{Cl}_{2(\text{g})} + e^- \rightleftharpoons \text{Cl}_{(\text{aq})}^-$ , with equilibrium potential  $U_{SHE}^\circ = 1.36 \text{ V}$ .<sup>72</sup> This reaction links an easy to calculate neutral gas-phase species,  $\text{Cl}_{2(\text{g})}$ , with the charged, difficult to model,  $\text{Cl}_{(\text{aq})}^-$ , allowing for the calculation of the free energy of the anion from that of the gas-phase species.<sup>61,64,65</sup> The CHE model<sup>59</sup> is an example of such an electrochemical thermodynamic cycle, but it is a special case where the equilibrium potential is defined to be exactly 0 V vs SHE at pH = 0, or 0 V vs RHE at all pH. In the method described here, we will show how to use such a cycle to determine the solution-phase free energy of ions using half-cell redox reactions that do not transfer the same number of protons and electrons.

A general representation of how to determine the free energy of solution-phase of charged species will be shown in the next sections, where we use reactions with a known experimental equilibrium potential, in two scenarios. The first is for reactions transferring electrons (with no proton transferred with the electrons), for instance, the  $\text{Cl}_2(\text{g})/\text{Cl}^-$  half-cell redox reaction, and the second for reactions transferring different numbers of protons and electrons, for instance the  $\text{SO}_4^{2-}(\text{aq})/\text{H}^+/\text{SO}_2(\text{aq})$ , half-cell redox reaction, where a different number of protons ( $4 \text{ H}^+$ ) and electrons ( $2 e^-$ ) participate in the reaction.

### 3.2.3 Half-cell redox couple with n electrons transferred

The following method has been described in the literature to calculate the free energy of an ion in solution to then construct adsorbate phase diagrams and determine adsorption potentials.<sup>64,65</sup> For the following generic reaction:



the change in free energy on a given potential scale is:

$$\Delta G = G_{A_{(\text{aq})}^{n-}} - \frac{1}{2}G_{A_{2(\text{g})}} + n|e_0|U \quad 3.5$$

At standard conditions and in the SHE scale, the free energy change is:

$$\Delta G^\circ = G_{A_{(\text{aq})}^{n-}}^\circ - \frac{1}{2}G_{A_{2(\text{g})}}^\circ + n|e_0|U_{SHE}^\circ \quad 3.6$$

where  $G_{A(aq)}^{n-}$ , is the standard solution-phase free energy of the anion,  $A_{(aq)}^{n-}$ .  $G_{A_2(g)}^{\circ}$ , is the standard gas-phase free energy of the neutral species,  $A_{2(g)}$ . The last term of Eq. 3.5,  $-n|e_0|U$ , is the free energy of the electrons participating in the reaction at an arbitrary potential scale,  $n$  is the number of electrons, and  $|e_0|$  is the elementary charge taken as positive. Eq. 3.6 is the free energy at standard conditions, and  $U_{SHE}^{\circ}$  is the electrode potential of the half-cell redox reaction on the SHE scale. Therefore, the free energy of the electrons at standard conditions is  $-n|e_0|U_{SHE}^{\circ}$ .

Note that at equilibrium, the change in the standard reaction free energy is equal to zero,  $\Delta G^{\circ} = 0$ , and the standard solution-phase free energy of the anion,  $G_{A(aq)}^{n-}$ , can be obtained from the standard gas-phase free energy,  $G_{A_2(g)}^{\circ}$ , and the experimentally measured equilibrium potential,  $U_{SHE}^{\circ}$ , taken from the standard electrode potential tables,<sup>72,73</sup> as shown in Eq. 3.7

$$G_{A(aq)}^{n-} = \frac{1}{2} G_{A_2(g)}^{\circ} - n|e_0|U_{SHE}^{\circ} \quad 3.7$$

At a different initial concentration of the anion, we can use the Nernst equation to obtain the anion solution-phase free energy at any concentration, important when comparing with experimental observations performed at non-standard state conditions, as done in reference<sup>66</sup> to determine the solution phase free energy of  $\text{Cl}^-$  (aq) and  $\text{ClO}_4^-$  (aq). The described approach can also be used to calculate the free energy of an aqueous cation, as shown by Akhade et al.<sup>78</sup>

### 3.2.4 Half-cell redox couples with unequal number of protons and electrons

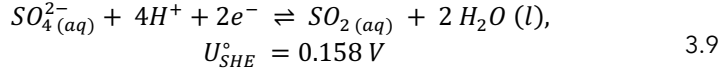
Many electrochemical reactions involve the transfer of both protons and electrons, sometimes in unequal numbers, to or from charged species. Since we can treat the free energy of ions and the energy of electrons independently, we can use the described method twice to calculate the free energy of an ion in a reaction involving protons (or for any other number of ions). The first calculation relates the free energy of protons to hydrogen gas at equilibrium, equivalent to the CHE approach,<sup>59</sup> and the second calculation computes the free energy of the ion of interest, as described above. This procedure can be repeated for any number of dissimilar ions in a given reaction. We can use this method with any reaction with (unequal) number of protons and electrons. Of course, the method works because at every calculation, we make use of an experimentally known equilibrium potential, as such avoiding the complicated and inaccurate calculation of the ion solvation energy.

In this method, the free energy of protons is described similarly as expressed in Eq. 3.7 for the generic redox couple ( $A_2/A^n$ ). In the particular case of the hydrogen half-redox reaction, ( $\text{H}^+/\text{H}_2$  (g)), the equilibrium potential is defined to be 0 V vs SHE and, therefore, the second term in Eq. 3.7 is zero, allowing us to

substitute the free energy of the protons for that of the DFT-calculated free energy of  $H_2(g)$ , as shown in Eq. 3.8, in a similar way as within the CHE framework.<sup>59</sup>

$$\frac{1}{2} G_{H_2(g)}^\circ = G_{H^+(aq)}^\circ \quad 3.8$$

As an example, we will show in a stepwise manner how to obtain the solution-phase free energy of  $SO_4^{2-}(aq)$  using a half-cell redox reaction that combines a neutral species  $SO_2(aq)$  with the charged  $SO_4^{2-}(aq)$  species, see Eq. 3.9. Note that the number of electrons and protons are different. The redox equation with its equilibrium potential<sup>72</sup> and the standard free energy are shown below:



$$\Delta G^\circ = G_{SO_2(aq)}^\circ + 2G_{H_2O(l)}^\circ - G_{SO_4^{2-}(aq)}^\circ - 4G_{H^+}^\circ + 2|e_0|(U_{SHE}^\circ) \quad 3.10$$

Eq. 3.10 is equal to zero,  $\Delta G^\circ = 0$ , when  $U$  is equal to  $U_{SHE}^\circ$ . By using Eq.3.8, and evaluating  $-n|e_0|U_{SHE}^\circ = -2|e_0|(0.158)V$  as shown in Eq. 3.11, we can calculate the standard solution-phase free energy of  $SO_4^{2-}(aq)$  in the SHE scale,  $G_{SO_4^{2-}(aq)}^\circ$  as shown in Eq. 3.12

$$\Delta G^\circ = G_{SO_2(aq)}^\circ + 2G_{H_2O(l)}^\circ - G_{SO_4^{2-}(aq)}^\circ - 2G_{H_2(g)}^\circ + 2e_0(0.158V)=0 \quad 3.11$$

$$G_{SO_4^{2-}(aq)}^\circ = G_{SO_2(aq)}^\circ + 2G_{H_2O(l)}^\circ - 2G_{H_2(g)}^\circ + 2e_0(0.158V) \quad 3.12$$

Now, the solution-phase free energy of the anion can be calculated from the free energy of neutral species, those of  $SO_2(g)$ ,  $H_2(g)$  and  $H_2O(g)$ . The free energy of water is obtained from that of  $H_2O(g)$  and corrected to that of liquid water. For  $SO_2(aq)$ , we did not include the correction and use the energy in the gas phase as the difference between the aqueous and gas-phase energies, based on experimental results, is almost zero (-0.005 eV) and does not significantly change the energy (see the computational methods section).

Similarly, other redox couple reactions could be used to obtain the solution-phase free energy of  $SO_4^{2-}(aq)$ , as shown in Figure 3.2 . For instance, the free energy of  $SO_4^{2-}(aq)$ , can also be determined from the equilibrium potentials of ( $S_2O_6^{2-}(aq)$ ,  $H^+ / SO_2(aq)$ ,  $U_{SHE}^\circ = 0.37V$ ) to determine the energy of  $S_2O_6^{2-}(aq)$  and then followed by ( $SO_4^{2-}(aq)$ ,  $H^+ / S_2O_6^{2-}(aq)$ ,  $U_{SHE}^\circ = -0.05V$ ) to then determine the solution-phase free energy of  $SO_4^{2-}(aq)$ .<sup>72</sup>

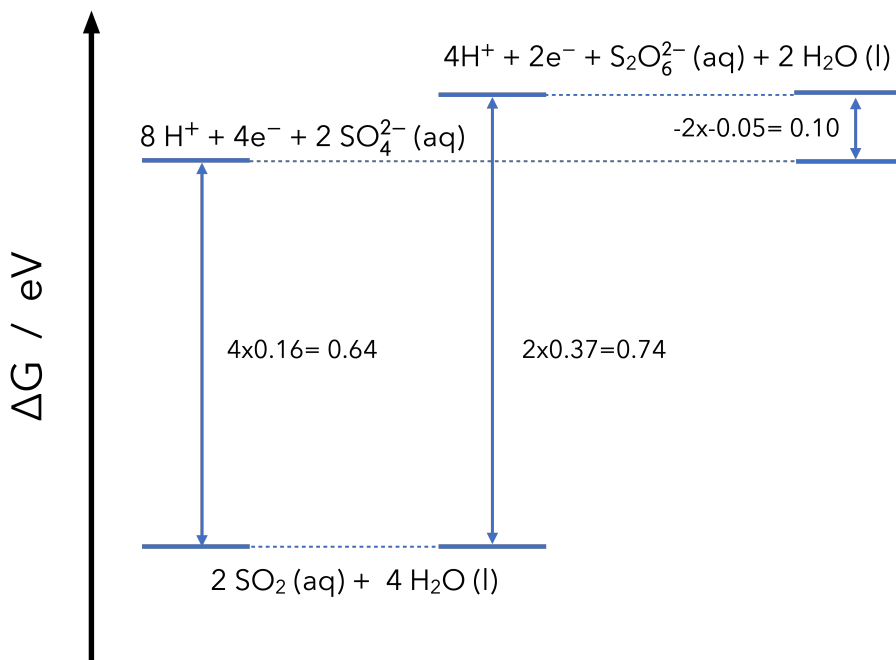
**FIGURE 3.2**

Illustration of electrochemical thermodynamic cycles that can be used to determine the solution-phase free energy of  $\text{SO}_4^{2-}(\text{aq})$  using the standard equilibrium potentials for  $[\text{SO}_4^{2-}(\text{aq}), \text{H}^+ / \text{SO}_2(\text{aq}), U_{SHE}^{\circ} = 0.158 \text{ V}]$ ,<sup>72</sup> or by combining  $[\text{S}_2\text{O}_6^{2-}(\text{aq}), \text{H}^+ / \text{SO}_2(\text{aq}), U_{SHE}^{\circ} = 0.37 \text{ V}]$ ,<sup>72</sup> and  $[\text{SO}_4^{2-}(\text{aq}), \text{H}^+ / \text{S}_2\text{O}_6^{2-}(\text{aq}), U_{SHE}^{\circ} = -0.05 \text{ V}]$ .<sup>72</sup>

### 3.3 Equilibrium adsorption energies and adsorption potentials

The solution-phase free energy of an ion is important in many areas of research and is particularly important for surface electrochemistry and (electro)catalysis, as the solution-phase free energy of an ion can be used to calculate adsorption thermodynamics and is necessary for comparing the adsorption strength between different species/adsorbates. These adsorption thermodynamics can be calculated relative to a neutral, gas-phase species such as  $\text{Cl}_2(\text{g})$  instead of  $\text{Cl}(\text{aq})$  (as described above), but this prohibits comparing adsorption strength from solution between different adsorbates (for example,  $\text{Cl}^*$  to  $\text{Br}^*$ ) as this comparison will require a correction of the gas-phase dissociation energy, ionization energy, and solvation energy for each adsorbate. It is important to be able to compare the adsorption strength between adsorbates as it allows the state, structure, and composition of the surface to be determined, for instance through a surface phase diagram.

In this section, we will show how to calculate the adsorption energy of an anion on any given surface site using the solution-phase free energy obtained using the method described here. The adsorption thermodynamics is calculated following

the reaction given in Eq. 3.13, where  $A_{(aq)}^{n-}$  represents a generic anion, (\*) a bare surface site, and  $A^*$  the adsorbed anion.



A similar reaction can be written for cation adsorption, with the electron written as a reactant instead of a product. Based on Eq. 3.13, we can write the change in free energy upon adsorption, shown in Eq. 3.14 (again, a similar equation can be written for cation adsorption):

$$\Delta G^{ads} = G_{A^*} - G_* - G_{A_{(aq)}^{n-}} - n|e_0|U_{SHE} \quad 3.14$$

where  $G_{A^*}$  is the free energy of the adsorbed species,  $G_*$  the free energy of the bare surface,  $G_{A_{(aq)}^{n-}}$  the free energy of the solution phase anion, and  $-n|e_0|U_{SHE}$  the free energy of the electrons transferred in the reaction at potential  $U_{SHE}$ , and the final adsorption energy can be shifted linearly with this term at an applied bias of interest to build, for instance, energy vs potential diagrams. Combining the CHE<sup>59</sup> approach with this method, we can add a term to Eq. 3.14 to consider the change in dipole moment induced by the adsorption of the charged species (\*A) on the surface (\*),  $\Delta\mu^{ads} = (\mu_{*A} - \mu_*)$ , and an additional term,  $(U_{SHE} - U_{PZC}/d)$ , to account for the dipole interaction with the electrode-electrolyte electric field. Based on the Helmholtz approximation of the double layer,<sup>59</sup>  $d$  is  $\sim 3.0 \text{ \AA}$  and we get Eq. 3.15

$$\Delta G_{*A}^{ads} = G_{A^*} - G_* - G_{A_{(aq)}^{n-}} - n|e_0|U_{SHE} + \Delta\mu^{ads} \frac{(U_{SHE} - U_{PZC})}{d} \quad 3.15$$

The potential of zero charge,  $U_{PZC}$ , is taken as the experimentally measured in the SHE scale.<sup>105</sup> Approximating the  $U_{PZC}$  to 0 V vs SHE does not significantly change the absolute adsorption potentials, see Table B3. This equation can then be solved for the equilibrium adsorption potential,  $U_{ads,SHE}^\circ$ , which represents the potential where adsorption becomes favorable (when  $\Delta G^{ads} = 0$ ), shown in Eq.3.16

$$U_{ads,SHE}^\circ = \frac{G_{*A} - G_{A^-(aq)} - G_* - \frac{\Delta\mu^{ads}}{d}U_{PZC}}{n|e_0| - \frac{\Delta\mu^{ads}}{d}} \quad 3.16$$

The potential scale on which this equilibrium adsorption potential sits depends on the methodology used to calculate the free energy of the ion in solution. Here, the standard hydrogen electrode scale is used. The free energy of the adsorbed species  $G_{A^*}$ , is calculated following Eq. 3.17:

$$G_{A^*} = E_{DFT} + ZPE - TS_{vib} \quad 3.17$$

where  $E_{DFT}$  is the 0 K DFT energy of the adsorbate on the surface, the  $ZPE$  is the zero-point vibrational energy, and  $S_{vib}$  is the vibrational entropy of the adsorbate. The free energy of the bare surface,  $G_*$ , is taken simply as the DFT energy at 0 K,

given that the vibrational energy/entropy of the surface is not significantly perturbed by the adsorbate.

### 3.4 Results and Discussion

#### 3.5 Applications of the method in electrocatalysis

To illustrate the use of this method in calculating relative adsorption strengths, we calculated the adsorption free energy at low coverage (1/9 ML) of iodide, bromide, chloride, and sulfate on Pt(111) and Au(111) and hydroxide on Pt(111). For comparison, we also calculated the adsorption free energy of Ag on Pt(111). From these adsorption free energies, we have calculated the equilibrium adsorption potential, the potential at which adsorption (at this coverage) becomes favorable, and plotted this against the experimentally measured adsorption potential. This is shown in Figure 3.3a, b).

From Figure 3.3a, b), it is clear that we can capture the relative trend in adsorption strength between each of these species, with the trend between the anions following  $I^* > Br^* > Cl^* > SO_4^* > OH^*$  across both surfaces. It is also apparent that all of the adsorbates bind less strongly on Au(111) than on Pt(111). This can be understood in terms of a more repulsive interaction between the adsorbates outer p-shells and the expanded d band of Au(111), compared to Pt(111), due to relativistic effects being more predominant on Au(111).<sup>106-108</sup> Furthermore, the d-band of Au(111) is more occupied than Pt(111).<sup>109</sup> This repulsive interaction also results in a longer bond length between the ions and the surface for ions adsorbed on Au(111) than on Pt(111), see Table B1. Of course, these trends were already known from experiment,<sup>110,111</sup> and agree well with prior computational calculations.<sup>107</sup>

We also examined the change in work function and the partial charges on the adsorbates with a Bader charge analysis, summarized in Table B1. We note that the analysis which includes solvation ( $SO_4^*$ -sol) considers only the change in work function associated with the single adsorbed water structures considered for the reactant ( $6H_2O^*$ ) and product ( $SO_4^*+4H_2O^*$ ) states. Our calculations follow the general trends found previously with DFT, see Groß et. al.,<sup>112-114</sup> Pašti et al.,<sup>109,115,116</sup> and Illas et al.<sup>107</sup> For Pt(111), we find a decrease in work function induced by the adsorption of Cl, Br, and I, and an increase induced by the adsorption of  $SO_4$ . In the case of Au(111), we see an increase in work function induced by the adsorption of Cl, Br and  $SO_4$  and a decrease induced by the adsorption of I.

Based on the Bader charge analysis, the adsorbates which retain more negative charge also induce a larger dipole moment (Table B1), and therefore they would benefit from solvation near the electrode surface to stabilize their energy. The general trend for induced dipole moment on both Pt(111) and Au(111) follows  $SO_4 > Cl > Br > I$ . The work function of Au(111) is smaller than that of Pt(111).<sup>117</sup> The higher the work function the less charge transfer, therefore the electronegative adsorbates on Au(111) will retain more negative charge than when adsorbed on Pt(111). The character of the halide bond on both Pt(111) and Au(111) has been conceptualized to be covalent in nature;<sup>118,114</sup> however, we can say that between the two, the bonding on Au(111) is slightly more ionic than on Pt(111), especially

for Cl, Br and SO<sub>4</sub>. In general, adsorbates that show higher charge separation tend to be more ionic in character,<sup>119</sup> but that is not always the case (as for instance Cl on Cu(111)<sup>120</sup>). Additional studies of electronic structure would be necessary to further investigate this.

The important result from Figure 3.3a , b) is that by using the method of determining the free energy of each ion in solution phase, at the same potential scale, we can reproduce the trends in adsorption potentials from DFT. We can now be confident in applying this method to understand more complex phenomena.

In general, we see good agreement between DFT and experiment when we include near-surface solvation for not only the trend in adsorption strength between adsorbates, but also the absolute value of the adsorption potentials. We can use Figure 3.3a , b) to make a few important points about this accuracy.

First, we note that we expect the calculated adsorption potential to be exchange-correlation functional dependent; the exact magnitude of the adsorption energy will vary with functional. If there is a significant difference in the van der Waals contribution to binding for these adsorbates between Pt(111) and Au(111), this could cause an additional dependence on functional, as traditional functionals poorly capture van der Waals interactions. However, we expect the trend between the adsorbates, differences between adsorption on Au(111) and Pt(111) (assuming the van der Waals contribution to binding is small), and the effect of near-surface solvation, to be less dependent on the chosen functional.

Second, it is interesting to see that by including only a few explicit water molecules hydrogen-bonded to the adsorbate, the adsorption potentials for SO<sub>4</sub><sup>\*</sup> on both Pt(111) and Au(111) as well as for OH<sup>\*</sup> on Pt(111) are brought much closer to those measured experimentally ( Figure 3.3a , b ) The mean and maximum absolute errors (MAE, MAX ) are MAE = 0.19 eV and MAX = 0.48 eV , compared to Figure 3.3a , b), where they are without solvation and the MAE = 0.33 eV and MAX= 0.76 eV and, therefore, far from the experimental results. This suggests that the influence of the rest of the water in the electrochemical environment, the second and third solvation shells of the adsorbate, might not further influence the stabilization of the adsorbate, as we already see a significant decrease in the MAE of about ~0.14 eV. Prior work by Calle-Vallejo et al.<sup>121,122</sup> and Janik et al.,<sup>123</sup> suggests that for many adsorbates, there is a threshold of number of explicit water molecules that will stabilize the energy of the adsorbate, and above that number, there is no significant impact. A wide variety of other methods for solvating the surface (implicit solvation, explicit solvation with classical or *ab-initio* molecular dynamics; for example) can be used in combination with the method we describe here to calculate the free energy of ions in solution, to further probe the effects of near-surface solvation on the adsorption energetics.

Third, it appears that the adsorption potentials on Au(111) are consistently underpredicted relative to experiment (at least for I<sup>\*</sup>, Br<sup>\*</sup>, and Cl<sup>\*</sup>), whereas this is not the case for Pt(111). Table B1 shows that the anions retain more negative charge (and create a larger change in surface-normal dipole moment on adsorption) on Au(111) than on Pt(111). We have included the dipole correction to the adsorption potential as calculated in Eq. 3.16, but this does not lead to a significant change in adsorption potential (Table B3), and so this alone cannot explain the difference in “accuracy” between Au(111) and Pt(111). We might expect, however, that the effect of near-surface solvation depends, at least in part, on the magnitude of the surface-normal dipole moment. As the halides retain more charge and generate a more positive surface normal dipole moment upon

adsorption on Au(111) than on Pt(111), we expect the effect of near-surface solvation on the adsorption of the halides, which we did not consider, to be larger on Au(111) than on Pt(111). In support of this idea, we can see that Figure 3.3a , b), where near-surface solvation is neglected (for all adsorbates), the calculated adsorption potential is equally far from the parity line for both Pt(111) and Au(111) for adsorbates which generate a more positive surface-normal dipole moment ( $\text{Cl}^*$ ,  $\text{SO}_4^*$ ). Additionally, we find the magnitude of the effect of solvation on the adsorption of  $\text{SO}_4^*$  (shifts adsorption potential by -0.27 V on Pt(111) and -0.68 V on Au(111)) proportional to the change in surface-normal dipole moment (0.47 eÅ on Pt(111), 0.82 eÅ on Au(111)).

We note that additional differences between Pt(111) and Au(111) could be due to a difference in the contribution of van der Waals interactions, which traditional exchange-correlation functionals poorly describe, as well as experimental factors; the experimentally measured potentials for anion adsorption on Au(111) were measured relative to the saturated calomel electrode (SCE), its potential on an SHE scale had to be assumed to shift these potentials to the same scale as those measured on Pt(111).

Lastly, the adsorption of some of the ions competes with that of other species (for example,  $\text{I}^*$  on Pt(111) with  $\text{H}^*$ , and  $\text{Ag}^*$  on Pt(111) with  $\text{SO}_4^*$ ), which would affect the measured adsorption potential; we have not considered this effect. Another factor, might be the use of experimental lattice constants, instead of DFT-converged lattice constants, due to the strain exerted on the slab, although we believe this to be a minor effect, it is good to keep in mind.

The preceding discussion makes it clear that the accuracy of the calculated adsorption potentials depends on a variety of factors including (i) the choice of exchange correlation functional (which influences both the energy of the reference gas-phase molecule to calculate the free energy of the ion in solution and the adsorption energy), (ii) the inclusion of near-surface solvation effects, (iii) co-adsorption, and (iv) the accuracy of the experimentally measured adsorption potential (including the choice and stability of the reference electrode). We mention these points here as they are important to understand how to model ion adsorption in the electrochemical environment, but each requires further study. Therefore, this *Chapter* is not intended as an evaluation of the accuracy of the method we have described here for calculating the free energy of solution-phase ions, only an example of its usefulness and simplicity.

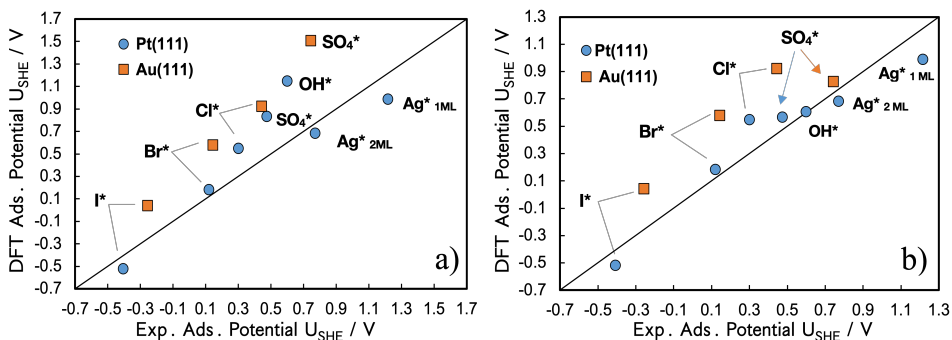


**FIGURE 3.3A, B)**

DFT simulated and experimentally measured equilibrium adsorption potential<sup>110,111,124</sup> of  $I^*$ ,  $Br^*$ ,  $Cl^*$ , and  $SO_4^*$  on Pt(111) and Au(111) as well as  $OH^*$  and the first and second monolayers of  $Ag^*$  on Pt(111). All potentials are simulated/measured at low coverage (1/9 ML), except for  $Ag^*$  on Pt(111) (for which the coverage is 1 and 2 ML). In (b), the adsorption potentials calculated for  $OH^*$  on Pt(111) and  $SO_4^*$  on Pt(111) and Au(111) include the effect of near-surface solvation, approximated by including co-adsorbed water molecules. The mean and maximum absolute errors (MAE and MAX) for (a) are (0.33, 0.76 eV) and for (b) are (0.19, 0.48 eV). Table B2 shows the calculated and experimentally measured adsorption potentials.

## 3.6 Conclusions

In this *Chapter* we have revised and illustrated a simple method that facilitates the calculation of solution-phase free energies of ions, eliminating the need to model solvation of the ions in bulk solution, and showed its importance by calculating adsorption potentials of different ions on the same potential scale. This is achieved by using an experimentally measured equilibrium potential to calculate the free energy of the ion in solution from a neutral gas-phase or solid-phase species. The method shows how the electrons and protons can be numerically arranged separately allowing to use any half-cell redox reaction.

We apply the method to examine the adsorption of a variety of different ions on Pt(111) and Au(111) and show the trend in adsorption strength matches the experimental trend. Our method is computationally efficient and its accuracy in terms of the energetics of the solution-phase charged species is only limited by how well DFT can model neutral gas-phase species and by the accuracy of the experimentally measured equilibrium potential of the reaction connecting the ion of interest to the neutral gas or solid-phase species. However, the accuracy of the calculated ion adsorption potential not only depends on the previous limitations but also by how well DFT can capture the effects of near-surface solvation, especially for adsorbates which induce a large surface-normal dipole moment, and the effects of a near-surface electric field.

The method used here is not new, however, we hope that by describing the methodology in detail and illustrating its usefulness, it will see more widespread use, such that the thermodynamics and kinetics of electrochemical and electrocatalytic reactions involving ions other than protons, will be more

frequently simulated with density functional theory. Such a method is necessary, for example, to examine the composition of a catalyst surface in electrochemical environments (surface phase diagram), competition in adsorption between species under reaction conditions, and the stability of an electrode or catalyst surface with respect to dissolution or (re)deposition; all examples at the forefront of computational electrocatalysis.

### 3.7 References

- (1) Hori, Y.; Koga, O.; Yamazaki, H.; Matsuo, T. Infrared Spectroscopy of Adsorbed CO and Intermediate Species in Electrochemical Reduction of CO<sub>2</sub> to Hydrocarbons on a Cu Electrode. *Electrochim. Acta* **1995**, *40* (16), 2617-2622.
- (2) Osawa, M. Dynamic Processes in Electrochemical Reactions Studied by Surface-Enhanced Infrared Absorption Spectroscopy (SEIRAS). *BCSJ* **1997**, *70* (12), 2861-2880.
- (3) Heinen, M.; Chen, Y. X.; Jusys, Z.; Behm, R. J. In Situ ATR-FTIRS Coupled with on-Line DEMS under Controlled Mass Transport Conditions—A Novel Tool for Electrocatalytic Reaction Studies. *Electrochim. Acta* **2007**, *52* (18), 5634-5643.
- (4) Neto, A. O.; Nandenha, J.; Assumpção, M. H. M. T.; Linardi, M.; Spinacé, E. V.; de Souza, R. F. B. In Situ Spectroscopy Studies of Ethanol Oxidation Reaction Using a Single Fuel Cell/ATR-FTIR Setup. *International Journal of Hydrogen Energy* **2013**, *38* (25), 10585-10591.
- (5) Pander, J. E.; Baruch, M. F.; Bocarsly, A. B. Probing the Mechanism of Aqueous CO<sub>2</sub> Reduction on Post-Transition-Metal Electrodes Using ATR-IR Spectroelectrochemistry. *ACS Catal.* **2016**, *6* (11), 7824-7833.
- (6) Wain, A. J.; O'Connell, M. A. Advances in Surface-Enhanced Vibrational Spectroscopy at Electrochemical Interfaces. *ADV PHYS-X* **2017**, *2* (1), 188-209.
- (7) Perales-Rondon, J. V.; Hernandez, S.; Martin-Yerga, D.; Fanjul-Bolado, P.; Heras, A.; Colina, A. Electrochemical Surface Oxidation Enhanced Raman Scattering. *Electrochim. Acta* **2018**, *282*, 377-383.
- (8) Baricuatro, J. H.; Kim, Y.-G.; Korzeniewski, C. L.; Soriaga, M. P. Tracking the Prelude of the Electroreduction of Carbon Monoxide via Its Interaction with Cu(100): Studies by Operando Scanning Tunneling Microscopy and Infrared Spectroscopy. *Catal. Today* **2020**, *358*, 210-214.
- (9) Zhu, Y.; Wang, J.; Chu, H.; Chu, Y.-C.; Chen, H. M. In Situ/Operando Studies for Designing Next-Generation Electrocatalysts. *ACS Energy Lett.* **2020**, *5* (4), 1281-1291.
- (10) Greeley, J.; Mavrikakis, M. Alloy Catalysts Designed from First Principles. *Nat. Mater.* **2004**, *3* (11), 810-815.
- (11) Greeley, J.; Jaramillo, T. F.; Bonde, J.; Chorkendorff, I.; Nørskov, J. K. Computational High-Throughput Screening of Electrocatalytic Materials for Hydrogen Evolution. *Nat. Mater.* **2006**, *5* (11), 909-913.
- (12) Magnussen, O. M.; Groß, A. Toward an Atomic-Scale Understanding of Electrochemical Interface Structure and Dynamics. *J. Am. Chem. Soc.* **2019**, *141* (12), 4777-4790.
- (13) Xin, H.; Linic, S. Communications: Exceptions to the d-Band Model of Chemisorption on Metal Surfaces: The Dominant Role of Repulsion between Adsorbate States and Metal d-States. *J. Chem. Phys.* **2010**, *132* (22), 221101.

- (14) Nørskov, J. K.; Abild-Pedersen, F.; Studt, F.; Bligaard, T. Density Functional Theory in Surface Chemistry and Catalysis. *PNAS* **2011**, *108* (3), 937-943.
- (15) Diaz-Morales, O.; Ledezma-Yanez, I.; Koper, M. T. M.; Calle-Vallejo, F. Guidelines for the Rational Design of Ni-Based Double Hydroxide Electrocatalysts for the Oxygen Evolution Reaction. *ACS Catal.* **2015**, *5* (9), 5380-5387.
- (16) Sakong, S.; Groß, A. The Electric Double Layer at Metal-Water Interfaces Revisited Based on a Charge Polarization Scheme. *J. Chem. Phys.* **2018**, *149* (8), 084705.
- (17) Schnur, S.; Groß, A. Challenges in the First-Principles Description of Reactions in Electrocatalysis. *Catal. Today* **2011**, *165* (1), 129-137.
- (18) Rossmeisl, J.; Skúlason, E.; Björketun, M. E.; Tripkovic, V.; Nørskov, J. K. Modeling the Electrified Solid-Liquid Interface. *Chem. Phys. Lett.* **2008**, *466* (1), 68-71.
- (19) Cohen, A. J.; Mori-Sánchez, P.; Yang, W. Insights into Current Limitations of Density Functional Theory. *Science* **2008**, *321* (5890), 792-794.
- (20) Lozovoi, A. Y.; Alavi, A.; Kohanoff, J.; Lynden-Bell, R. M. Ab Initio Simulation of Charged Slabs at Constant Chemical Potential. *J. Chem. Phys.* **2001**, *115* (4), 1661-1669.
- (21) Filhol, J.-S.; Neurock, M. Elucidation of the Electrochemical Activation of Water over Pd by First Principles. *Angew. Chem. Int. Ed.* **2006**, *45* (3), 402-406.
- (22) Taylor, C. D.; Wasileski, S. A.; Filhol, J.-S.; Neurock, M. First Principles Reaction Modeling of the Electrochemical Interface: Consideration and Calculation of a Tunable Surface Potential from Atomic and Electronic Structure. *Phys. Rev. B* **2006**, *73* (16), 165402.
- (23) A. Gauthier, J.; D. Chen, L.; Bajdich, M.; Chan, K. Implications of the Fractional Charge of Hydroxide at the Electrochemical Interface. *Phys. Chem. Chem. Phys.* **2020**, *22* (13), 6964-6969.
- (24) Tölle, J.; Gomes, A. S. P.; Ramos, P.; Pavanello, M. Charged-Cell Periodic DFT Simulations via an Impurity Model Based on Density Embedding: Application to the Ionization Potential of Liquid Water. *Int. J. Quantum Chem.* **2019**, *119* (1), e25801.
- (25) Schnur, S.; Groß, A. Properties of Metal-Water Interfaces Studied from First Principles. *New J. Phys.* **2009**, *11* (12), 125003.
- (26) Desai, S. K.; Pallassana, V.; Neurock, M. A Periodic Density Functional Theory Analysis of the Effect of Water Molecules on Deprotonation of Acetic Acid over Pd(111). *J. Phys. Chem. B* **2001**, *105* (38), 9171-9182.
- (27) Gauthier, J. A.; Dickens, C. F.; Chen, L. D.; Doyle, A. D.; Nørskov, J. K. Solvation Effects for Oxygen Evolution Reaction Catalysis on IrO<sub>2</sub>(110). *J. Phys. Chem. C* **2017**, *121* (21), 11455-11463.
- (28) Kimmel, G. A.; Matthiesen, J.; Baer, M.; Mundy, C. J.; Petrik, N. G.; Smith, R. S.; Dohnálek, Z.; Kay, B. D. No Confinement Needed: Observation of a Metastable Hydrophobic Wetting Two-Layer Ice on Graphene. *J. Am. Chem. Soc.* **2009**, *131* (35), 12838-12844.
- (29) Gunathunge, C. M.; Ovalle, V. J.; Li, Y.; Janik, M. J.; Waagele, M. M. Existence of an Electrochemically Inert CO Population on Cu Electrodes in Alkaline PH. *ACS Catal.* **2018**, *8* (8), 7507-7516.
- (30) Tripkovic, V. Thermodynamic Assessment of the Oxygen Reduction Activity in Aqueous Solutions. *Phys. Chem. Chem. Phys.* **2017**, *19* (43), 29381-29388.
- (31) Shan, N.; Liu, B. Elucidating Molecular Interactions in Glycerol Adsorption at the Metal-Water Interface with Density Functional Theory. *Langmuir* **2019**, *35* (14), 4791-4805.
- (32) Granda-Marulanda, L. P.; Builes, S.; Koper, M. T. M.; Calle-Vallejo, F. Influence of Van Der Waals Interactions on the Solvation Energies of Adsorbates at Pt-Based Electrocatalysts. *ChemPhysChem* **2019**, *20* (22), 2968-2972.

- (33) Ringe, S.; Oberhofer, H.; Hille, C.; Matera, S.; Reuter, K. Function-Space-Based Solution Scheme for the Size-Modified Poisson–Boltzmann Equation in Full-Potential DFT. *J. Chem. Theory Comput.* **2016**, *12* (8), 4052–4066.
- (34) Mathew, K.; Sundararaman, R.; Letchworth-Weaver, K.; Arias, T. A.; Hennig, R. G. Implicit Solvation Model for Density-Functional Study of Nanocrystal Surfaces and Reaction Pathways. *J. Chem. Phys.* **2014**, *140* (8), 084106.
- (35) Schwarz, K. A.; Sundararaman, R.; Moffat, T. P.; Allison, T. C. Formic Acid Oxidation on Platinum: A Simple Mechanistic Study. *Phys. Chem. Chem. Phys.* **2015**, *17* (32), 20805–20813.
- (36) Sakong, S.; Groß, A. The Importance of the Electrochemical Environment in the Electro-Oxidation of Methanol on Pt(111). *ACS Catal.* **2016**, *6* (8), 5575–5586.
- (37) Weitzner, S. E.; Akhade, S. A.; Varley, J. B.; Wood, B. C.; Otani, M.; Baker, S. E.; Duoss, E. B. Toward Engineering of Solution Microenvironments for the CO<sub>2</sub> Reduction Reaction: Unraveling PH and Voltage Effects from a Combined Density-Functional-Continuum Theory. *J. Phys. Chem. Lett.* **2020**, *11* (10), 4113–4118.
- (38) Qiao, C.; Zhang, J.; Jiang, P.; Zhao, S.; Song, X.; Yu, J. A Molecular Approach for Predicting Phase Diagrams of Ternary Aqueous Saline Solutions. *Chem. Eng. Sci.* **2020**, *211*, 115278.
- (39) Brancato, G.; Rega, N.; Barone, V. A Hybrid Explicit/Implicit Solvation Method for First-Principle Molecular Dynamics Simulations. *J. Chem. Phys.* **2008**, *128* (14), 144501.
- (40) Sakong, S.; Naderian, M.; Mathew, K.; Hennig, R. G.; Groß, A. Density Functional Theory Study of the Electrochemical Interface between a Pt Electrode and an Aqueous Electrolyte Using an Implicit Solvent Method. *The Journal of Chemical Physics* **2015**, *142* (23), 234107.
- (41) Ge, X.; Wang, J.; Zhang, Z.; Wang, X.; Chen, M. Thermodynamic Modeling of Electrolyte Solutions by a Hybrid Ion-Interaction and Solvation (HIS) Model. *Calphad* **2015**, *48*, 79–88.
- (42) Spohr, E. Computer Simulation of the Water/Platinum Interface. *J. Phys. Chem.* **1989**, *93* (16), 6171–6180.
- (43) Li, X.; Ågren, H. Molecular Dynamics Simulations Using a Capacitance-Polarizability Force Field. *J. Phys. Chem. C* **2015**, *119* (33), 19430–19437.
- (44) Steinmann, S. N.; Ferreira De Morais, R.; Götz, A. W.; Fleurat-Lessard, P.; Iannuzzi, M.; Sautet, P.; Michel, C. Force Field for Water over Pt(111): Development, Assessment, and Comparison. *J. Chem. Theory Comput.* **2018**, *14* (6), 3238–3251.
- (45) Sundararaman, R.; Schwarz, K. Evaluating Continuum Solvation Models for the Electrode-Electrolyte Interface: Challenges and Strategies for Improvement. *The Journal of Chemical Physics* **2017**, *146* (8), 084111.
- (46) N. Steinmann, S.; Sautet, P.; Michel, C. Solvation Free Energies for Periodic Surfaces: Comparison of Implicit and Explicit Solvation Models. *Phys. Chem. Chem. Phys.* **2016**, *18* (46), 31850–31861.
- (47) Gauthier, J. A.; Ringe, S.; Dickens, C. F.; Garza, A. J.; Bell, A. T.; Head-Gordon, M.; Nørskov, J. K.; Chan, K. Challenges in Modeling Electrochemical Reaction Energetics with Polarizable Continuum Models. *ACS Catal.* **2019**, *9* (2), 920–931.
- (48) Marenich, A. V.; Cramer, C. J.; Truhlar, D. G. Universal Solvation Model Based on Solute Electron Density and on a Continuum Model of the Solvent Defined by the Bulk Dielectric Constant and Atomic Surface Tensions. *J. Phys. Chem. B* **2009**, *113* (18), 6378–6396.

- (49) Kelly, C. P.; Cramer, C. J.; Truhlar, D. G. Aqueous Solvation Free Energies of Ions and Ion–Water Clusters Based on an Accurate Value for the Absolute Aqueous Solvation Free Energy of the Proton. *J. Phys. Chem. B* **2006**, *110* (32), 16066–16081.
- (50) Marković, Z.; Tošović, J.; Milenković, D.; Marković, S. Revisiting the Solvation Enthalpies and Free Energies of the Proton and Electron in Various Solvents. *Comput. Theor. Chem.* **2016**, *1077*, 11–17.
- (51) Malloum, A.; Fifen, J. J.; Conradie, J. Solvation Energies of the Proton in Methanol Revisited and Temperature Effects. *Phys. Chem. Chem. Phys.* **2018**, *20* (46), 29184–29206.
- (52) Zhan, C.-G.; Dixon, D. A. First-Principles Determination of the Absolute Hydration Free Energy of the Hydroxide Ion. *J. Phys. Chem. A* **2002**, *106* (42), 9737–9744.
- (53) Bryantsev, V. S.; Diallo, M. S.; Goddard III, W. A. Calculation of Solvation Free Energies of Charged Solutes Using Mixed Cluster/Continuum Models. *J. Phys. Chem. B* **2008**, *112* (32), 9709–9719.
- (54) Dupont, C.; Andreussi, O.; Marzari, N. Self-Consistent Continuum Solvation (SCCS): The Case of Charged Systems. *J. Chem. Phys.* **2013**, *139* (21), 214110.
- (55) Pliego, J. R. Thermodynamic Cycles and the Calculation of PKa. *Chem. Phys. Lett.* **2003**, *367* (1), 145–149.
- (56) Ho, J. Are Thermodynamic Cycles Necessary for Continuum Solvent Calculation of PKas and Reduction Potentials? *Phys. Chem. Chem. Phys.* **2014**, *17* (4), 2859–2868.
- (57) Wang, C.; Ren, P.; Luo, R. Ionic Solution: What Goes Right and Wrong with Continuum Solvation Modeling. *J. Phys. Chem. B* **2017**, *121* (49), 11169–11179.
- (58) Stein, C. J.; Herbert, J. M.; Head-Gordon, M. The Poisson–Boltzmann Model for Implicit Solvation of Electrolyte Solutions: Quantum Chemical Implementation and Assessment via Sechenov Coefficients. *J. Chem. Phys.* **2019**, *151* (22), 224111.
- (59) Nørskov, J. K.; Rossmeisl, J.; Logadottir, A.; Lindqvist, L.; Kitchin, J. R.; Bligaard, T.; Jónsson, H. Origin of the Overpotential for Oxygen Reduction at a Fuel-Cell Cathode. *J. Phys. Chem. B* **2004**, *108* (46), 17886–17892.
- (60) Calle-Vallejo, F.; Huang, M.; Henry, J. B.; Koper, M. T. M.; Bandarenka, A. S. Theoretical Design and Experimental Implementation of Ag/Au Electrodes for the Electrochemical Reduction of Nitrate. *Phys. Chem. Chem. Phys.* **2013**, *15* (9), 3196–3202.
- (61) McCrum, I. T.; Akhade, S. A.; Janik, M. J. Electrochemical Specific Adsorption of Halides on Cu 111, 100, and 211: A Density Functional Theory Study. *Electrochim. Acta* **2015**, *173*, 302–309.
- (62) Yeh, K.-Y.; Restaino, N. A.; Esopi, M. R.; Maranas, J. K.; Janik, M. J. The Adsorption of Bisulfate and Sulfate Anions over a Pt(111) Electrode: A First Principle Study of Adsorption Configurations, Vibrational Frequencies and Linear Sweep Voltammogram Simulations. *Catal. Today* **2013**, *202*, 20–35.
- (63) Trasatti, S. The Absolute Electrode Potential: An Explanatory Note (Recommendations 1986). *Pure Appl. Chem.* **1986**, *58* (7), 955–966.
- (64) Hansen, H. A.; Man, I. C.; Studt, F.; Abild-Pedersen, F.; Bligaard, T.; Rossmeisl, J. Electrochemical Chlorine Evolution at Rutile Oxide (110) Surfaces. *Phys. Chem. Chem. Phys.* **2009**, *12* (1), 283–290.
- (65) Gossenberger, F.; Roman, T.; Groß, A. Hydrogen and Halide Co-Adsorption on Pt(111) in an Electrochemical Environment: A Computational Perspective. *Electrochim. Acta* **2016**, *216*, 152–159.
- (66) Bondarenko, A. S.; Stephens, I. E. L.; Hansen, H. A.; Pérez-Alonso, F. J.; Tripkovic, V.; Johansson, T. P.; Rossmeisl, J.; Nørskov, J. K.; Chorkendorff, I. The Pt(111)/Electrolyte

- Interface under Oxygen Reduction Reaction Conditions: An Electrochemical Impedance Spectroscopy Study. *Langmuir* **2011**, *27* (5), 2058–2066.
- (67) Gossenberger, F.; Juarez, F.; Groß, A. Sulfate, Bisulfate, and Hydrogen Co-Adsorption on Pt(111) and Au(111) in an Electrochemical Environment. *Front. Chem.* **2020**, *8*.
- (68) Harima, Y. Standard Potential and Chemical Solvation Energy of an Electron in Ethylenediamine. *J. Electroanal. Chem. Interf. Electrochem.* **1988**, *252* (1), 53–60.
- (69) Marenich, A. V.; Ho, J.; Coote, M. L.; Cramer, C. J.; Truhlar, D. G. Computational Electrochemistry: Prediction of Liquid-Phase Reduction Potentials. *Phys. Chem. Chem. Phys.* **2014**, *16* (29), 15068–15106.
- (70) J. Göttle, A.; M. Koper, M. T. Proton-Coupled Electron Transfer in the Electrocatalysis of CO<sub>2</sub> Reduction: Prediction of Sequential vs. Concerted Pathways Using DFT. *Chem. Sci.* **2017**, *8* (1), 458–465.
- (71) Kepp, K. P. Thermochemically Consistent Free Energies of Hydration for Di- and Trivalent Metal Ions. *J. Phys. Chem. A* **2018**, *122* (37), 7464–7471.
- (72) Bratsch, S. G. Standard Electrode Potentials and Temperature Coefficients in Water at 298.15 K. *J. Phys. Chem. Ref. Data* **1989**, *18* (1), 1–21.
- (73) Lide, D. R. CRC Handbook of Chemistry and Physics, 85th Edition; CRC Press, 2004.
- (74) Seitz, L. C.; Dickens, C. F.; Nishio, K.; Hikita, Y.; Montoya, J.; Doyle, A.; Kirk, C.; Vojvodic, A.; Hwang, H. Y.; Norskov, J. K.; Jaramillo, T. F. A Highly Active and Stable IrOx/SrIrO<sub>3</sub> Catalyst for the Oxygen Evolution Reaction. *Science* **2016**, *353* (6303), 1011–1014.
- (75) Strmcnik, D.; Kodama, K.; Vliet, D. van der; Greeley, J.; Stamenkovic, V. R.; Marković, N. M. The Role of Non-Covalent Interactions in Electrocatalytic Fuel-Cell Reactions on Platinum. *Nature Chem* **2009**, *1* (6), 466–472.
- (76) Stoffelsma, C.; Rodriguez, P.; Garcia, G.; Garcia-Araez, N.; Strmcnik, D.; Marković, N. M.; Koper, M. T. M. Promotion of the Oxidation of Carbon Monoxide at Stepped Platinum Single-Crystal Electrodes in Alkaline Media by Lithium and Beryllium Cations. *J. Am. Chem. Soc.* **2010**, *132* (45), 16127–16133.
- (77) Colic, V.; Pohl, M. D.; Scieszka, D.; Bandarenka, A. S. Influence of the Electrolyte Composition on the Activity and Selectivity of Electrocatalytic Centers. *Catal. Today* **2016**, *262*, 24–35.
- (78) Akhade, S. A.; McCrum, I. T.; Janik, M. J. The Impact of Specifically Adsorbed Ions on the Copper-Catalyzed Electroreduction of CO<sub>2</sub>. *J. Electrochem. Soc.* **2016**, *163* (6), F477.
- (79) McCrum, I. T.; Janik, M. J. First Principles Simulations of Cyclic Voltammograms on Stepped Pt(553) and Pt(533) Electrode Surfaces. *ChemElectroChem* **2016**, *3* (10), 1609–1617.
- (80) Ringe, S.; Clark, E. L.; Resasco, J.; Walton, A.; Seger, B.; Bell, A. T.; Chan, K. Understanding Cation Effects in Electrochemical CO<sub>2</sub> Reduction. *Energy Environ. Sci.* **2019**, *12* (10), 3001–3014.
- (81) Waegele, M. M.; Gunathunge, C. M.; Li, J.; Li, X. How Cations Affect the Electric Double Layer and the Rates and Selectivity of Electrocatalytic Processes. *J. Chem. Phys.* **2019**, *151* (16), 160902.
- (82) Gauthier, J. A.; Fields, M.; Bajdich, M.; Chen, L. D.; Sandberg, R. B.; Chan, K.; Nørskov, J. K. Facile Electron Transfer to CO<sub>2</sub> during Adsorption at the Metal|Solution Interface. *J. Phys. Chem. C* **2019**, *123* (48), 29278–29283.
- (83) Kristoffersen, H. H.; Chan, K.; Vegge, T.; Hansen, H. A. Energy–Entropy Competition in Cation–Hydroxyl Interactions at the Liquid Water–Pt(111) Interface. *Chem. Commun.* **2020**, *56* (3), 427–430.
- (84) Kresse, G.; Furthmüller, J. Efficient Iterative Schemes for Ab Initio Total-Energy Calculations Using a Plane-Wave Basis Set. *Phys. Rev. B* **1996**, *54* (16), 11169–11186.

- (85) Kresse, G.; Furthmüller, J. Efficiency of Ab-Initio Total Energy Calculations for Metals and Semiconductors Using a Plane-Wave Basis Set. *Comput. Mater. Sci.* **1996**, *6* (1), 15-50.
- (86) Kresse, G. Ab Initio Molecular Dynamics for Liquid Metals. *J. Non-Cryst. Solids* **1995**, *192-193*, 222-229.
- (87) Blöchl, P. E. Projector Augmented-Wave Method. *Phys. Rev. B* **1994**, *50* (24), 17953-17979.
- (88) Kresse, G.; Joubert, D. From ultrasoft pseudopotentials to the projector augmented-wave method. *Phys. Rev. B* **1999**, *59* (3), 1758-1775.
- (89) Perdew, J. P.; Burke, K.; Ernzerhof, M. Generalized Gradient Approximation Made Simple. *Phys. Rev. Lett.* **1996**, *77* (18), 3865-3868.
- (90) Perdew, J. P.; Burke, K.; Ernzerhof, M. Perdew, Burke, and Ernzerhof Reply: *Phys. Rev. Lett.* **1998**, *80* (4), 891-891.
- (91) Charles Kittel. Introduction to Solid State Physics, 7th Edition | Wiley; 2004.
- (92) Monkhorst, H. J.; Pack, J. D. Special Points for Brillouin-Zone Integrations. *Phys. Rev. B* **1976**, *13* (12), 5188-5192.
- (93) Bengtsson, L. Dipole Correction for Surface Supercell Calculations. *Phys. Rev. B* **1999**, *59* (19), 12301-12304.
- (94) Singh-Miller, N. E.; Marzari, N. Surface Energies, Work Functions, and Surface Relaxations of Low-Index Metallic Surfaces from First Principles. *Phys. Rev. B* **2009**, *80* (23), 235407.
- (95) Calle-Vallejo, F.; Koper, M. T. M. First-Principles Computational Electrochemistry: Achievements and Challenges. *Electrochim. Acta* **2012**, *84*, 3-11.
- (96) Goldberg, R. N.; Parker, V. B. *Thermodynamics of Solution of SO<sub>2</sub>(g) in Water and of Aqueous Sulfur Dioxide Solutions*; PB-86-166808/XAB; National Bureau of Standards, Washington, DC (USA), 1985.
- (97) Bader, R. F. W. *Atoms in Molecules: A Quantum Theory*; Clarendon Press: Oxford, 1994.
- (98) Bader, R. F. W. Atoms in Molecules. *Acc. Chem. Res.* **1985**, *18* (1), 9-15.
- (99) Henkelman, G.; Arnaldsson, A.; Jónsson, H. A Fast and Robust Algorithm for Bader Decomposition of Charge Density. *Ojha, K* **2006**, *36* (3), 354-360.
- (100) Baxter, G. P.; Hickey, C. H.; Holmes, W. C. THE VAPOR PRESSURE OF IODINE. *J. Am. Chem. Soc.* **1907**, *29* (2), 127-136.
- (101) Peterson, A. A.; Abild-Pedersen, F.; Studt, F.; Rossmeisl, J.; Nørskov, J. K. How Copper Catalyzes the Electroreduction of Carbon Dioxide into Hydrocarbon Fuels. *Energy Environ. Sci.* **2010**, *3* (9), 1311-1315.
- (102) Christensen, R.; Hansen, H. A.; Vegge, T. Identifying Systematic DFT Errors in Catalytic Reactions. *Catal. Sci. Technol.* **2015**, *5* (11), 4946-4949.
- (103) Granda-Marulanda, L. P.; Rendón-Calle, A.; Builes, S.; Illas, F.; Koper, M. T. M.; Calle-Vallejo, F. A Semiempirical Method to Detect and Correct DFT-Based Gas-Phase Errors and Its Application in Electrocatalysis. *ACS Catal.* **2020**, *10* (12), 6900-6907.
- (104) Persson, K. A.; Waldwick, B.; Lazic, P.; Ceder, G. Prediction of Solid-Aqueous Equilibria: Scheme to Combine First-Principles Calculations of Solids with Experimental Aqueous States. *Phys. Rev. B* **2012**, *85* (23), 235438.
- (105) Ojha, K.; Arulmozhi, N.; Aranzales, D.; Koper, M. T. M. Double Layer at the Pt(111)-Aqueous Electrolyte Interface: Potential of Zero Charge and Anomalous Gouy-Chapman Screening. *Angew. Chem. Int. Ed.* **2020**, *59* (2), 711-715.
- (106) Autschbach, J. Perspective: Relativistic Effects. *J. Chem. Phys.* **2012**, *136* (15), 150902.
- (107) Migani, A.; Illas, F. A Systematic Study of the Structure and Bonding of Halogens on Low-Index Transition Metal Surfaces. *J. Phys. Chem. B* **2006**, *110* (24), 11894-11906.

- (108) Hammer, B.; Norskov, J. K. Why Gold Is the Noblest of All the Metals. *Nature* **1995**, 376 (6537), 238-240.
- (109) Pašti, I. A.; Mentus, S. V. Halogen Adsorption on Crystallographic (111) Planes of Pt, Pd, Cu and Au, and on Pd-Monolayer Catalyst Surfaces: First-Principles Study. *Electrochim. Acta* **2010**, 55 (6), 1995-2003.
- (110) Garcia-Araez, N.; Climent, V.; Herrero, E.; Feliu, J.; Lipkowski, J. Thermodynamic Studies of Bromide Adsorption at the Pt(111) Electrode Surface Perchloric Acid Solutions: Comparison with Other Anions. *J. Electroanal. Chem.* **2006**, 591 (2), 149-158.
- (111) Lipkowski, J.; Shi, Z.; Chen, A.; Pettinger, B.; Bilger, C. Ionic Adsorption at the Au(111) Electrode. *Electrochim. Acta* **1998**, 43 (19), 2875-2888.
- (112) Roman, T.; Groß, A. Periodic Density-Functional Calculations on Work-Function Change Induced by Adsorption of Halogens on Cu(111). *Phys. Rev. Lett.* **2013**, 110 (15), 156804.
- (113) Gossenberger, F.; Roman, T.; Forster-Tonigold, K.; Groß, A. Change of the Work Function of Platinum Electrodes Induced by Halide Adsorption. *Beilstein J Nanotechnol* **2014**, 5, 152-161.
- (114) Roman, T.; Gossenberger, F.; Forster-Tonigold, K.; Groß, A. Halide Adsorption on Close-Packed Metal Electrodes. *Phys. Chem. Chem. Phys.* **2014**, 16 (27), 13630-13634.
- (115) Pašti, I.; Gavrilov, N.; Mentus, S. Fluorine Adsorption on Transition Metal Surfaces: A DFT Study. *J. Serbian Chem. Soc.* **2013**, 78 (11), 1763-1773.
- (116) Pašti, I. A.; Gavrilov, N. M.; Mentus, S. V. DFT Study of Chlorine Adsorption on Bimetallic Surfaces - Case Study of Pd<sub>3</sub>M and Pt<sub>3</sub>M Alloy Surfaces. *Electrochim. Acta* **2014**, 130, 453-463.
- (117) Derry, G. N.; Kern, M. E.; Worth, E. H. Recommended Values of Clean Metal Surface Work Functions. *J. Vac. Sci. Technol. A* **2015**, 33 (6), 060801.
- (118) Baker, T. A.; Friend, C. M.; Kaxiras, E. Nature of Cl Bonding on the Au(111) Surface: Evidence of a Mainly Covalent Interaction. *J. Am. Chem. Soc.* **2008**, 130 (12), 3720-3721.
- (119) Oliveira, V.; Cremer, D. Transition from Metal-Ligand Bonding to Halogen Bonding Involving a Metal as Halogen Acceptor a Study of Cu, Ag, Au, Pt, and Hg Complexes. *Chem. Phys. Lett.* **2017**, 681, 56-63.
- (120) Peljhan, S.; Kokalj, A. Adsorption of Chlorine on Cu(111): A Density-Functional Theory Study. *J. Phys. Chem. C* **2009**, 113 (32), 14363-14376.
- (121) Calle-Vallejo, F.; F. de Moraes, R.; Illas, F.; Loffreda, D.; Sautet, P. Affordable Estimation of Solvation Contributions to the Adsorption Energies of Oxygenates on Metal Nanoparticles. *J. Phys. Chem. C* **2019**, 123 (9), 5578-5582.
- (122) Rendón-Calle, A.; Builes, S.; Calle-Vallejo, F. Substantial Improvement of Electrocatalytic Predictions by Systematic Assessment of Solvent Effects on Adsorption Energies. *Appl. Catal. B* **2020**, 276, 119147.
- (123) Mills, J. N.; McCrum, I. T.; Janik, M. J. Alkali Cation Specific Adsorption onto Fcc(111) Transition Metal Electrodes. *Phys. Chem. Chem. Phys.* **2014**, 16 (27), 13699-13707.
- (124) Hachiya, T.; Itaya, K. In Situ Scanning Tunneling Microscopy of Underpotential Deposition in Aqueous Solution III. Silver Adlayers on Au(111). *Ultramicroscopy* **1992**, 42-44, 445-452.